# Sensors & Diagnostics

Check for updates

# Si–rhodamine derivative with a large stokes shift for ELISA-based detection of SARS-CoV-2†

Yan-Hong Liu,‡[a] Hong Zhang,‡[a] Kang-Kang Yu, [iD][a] Xiao-Fang Pei,[b] Jia-Nan Xu,[c] Shan-Yong Chen, [iD][a] Xiao-Qi Yu [iD][a] and Kun Li [iD]*[a]

In view of the worldwide impact of SARS-CoV-2, developing rapid and accurate ELISA-based methods for detecting SARS-CoV-2 is of great importance for diagnosing and controlling coronavirus disease 2019. Herein, we report highly stable and fluorescently bright Si–rhodamine analogues with obviously improved Stokes shifts for IgG antibody labelling. These new fluorescent dye labels provide a promising fluorescence tool for SARS-Cov-2 detection.

Severe acute respiratory syndrome coronavirus 2 (SARS-CoV-2), which causes coronavirus disease 2019 (COVID 19), has spread widely all over the world, infecting millions of people and causing a human pandemic.[1–4] How to precisely differentiate COVID-19 patients from healthy people is a difficult problem and an emergency.[5–7] Currently, several methods serve as the primary tools for achieving clinical diagnosis of the infection, including virus nucleic acid real-time polymerase chain reaction (RT-PCR), CT imaging, and antibody testing.[5,6,8,9] Although the RT-PCR test has become the standard diagnostic method for the diagnosis of COVID-19, it suffers from the need to use certified laboratories, long turnaround time and complicated operation,[10] as well as the need to use trained technicians to operate the expensive equipment in order to avoid false negatives.[5,11–14] Therefore, it is urgent to develop a rapid, simple-to-use, sensitive, and accurate test for identifying infected patients.

The enzyme-linked immunosorbent assay (ELISA) is a rapid detection method that utilizes the specific reaction between antigen and antibody with high precision and good accuracy.[11–15] Several serological immunoassays have been developed for detecting SARS-CoV-2 viral proteins and antibodies in serum or plasma, in which the spike protein (SP), receptor binding domain (RBD) and nucleocapsid protein (NP) appear to be the main targets.[5,11,12] As the key parameter (fluorescence signal) for sensing activity, fluorescent dyes that display good photophysical properties and anti-interference ability are important for labelling secondary antibodies. FITC, RRX, Cy3(5), PE are dyes widely used for labelling IgG antibodies, but show small Stokes shifts and are easily interfered with by GSH in serum, resulting in false positives.[16] Therefore, developing fluorescent dyes with large Stokes shifts and strong anti-interference abilities is extremely important.

[a] *Key Laboratory of Green Chemistry and Technology (Ministry of Education) College of Chemistry, Sichuan University, 29 Wangjiang Road Chengdu, 610064, P. R. China. E-mail: kli@scu.edu.cn*

[b] *West China School of Public Health, Sichuan University 16#, Section 3, Renmin Nan Lu Chengdu, Sichuan 610041, P. R. China*

[c] *Sichuan Center for Disease Control and Prevention, No. 6 Zhongxue Road, Chengdu, 610041, P. R. China*

† Electronic supplementary information (ESI) available. See DOI: https://doi.org/10.1039/d4sd00038b

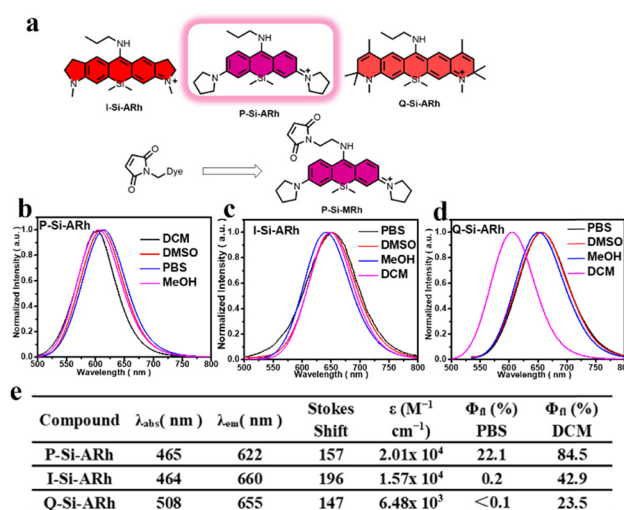‡ These authors contributed equally to this work.

Fig. 1 (a) Chemical structures of SiRh analogues (b)–(d) fluorescence spectra of SiRh analogues in indicated solvents. (e) Summary of photophysical properties of SiRh analogues at 25 °C in PBS pH 7.4 solutions. The concentrations of the dyes were 10 μM. $\lambda_{abs}$ = absorption wavelength, $\lambda_{em}$ = emission wavelength, $\varepsilon$ = molar extinction coefficient, $\Phi$ = fluorescence quantum yield.

| Compound | $\lambda_{abs}$ (nm) | $\lambda_{em}$ (nm) | Stokes Shift | $\varepsilon$ ($M^{-1}$ $cm^{-1}$) | $\Phi_{fl}$ (%) PBS | $\Phi_{fl}$ (%) DCM |
|---|---|---|---|---|---|---|
| P-Si-ARh | 465 | 622 | 157 | $2.01 \times 10^4$ | 22.1 | 84.5 |
| I-Si-ARh | 464 | 660 | 196 | $1.57 \times 10^4$ | 0.2 | 42.9 |
| Q-Si-ARh | 508 | 655 | 147 | $6.48 \times 10^3$ | <0.1 | 23.5 |

In recent years, xanthene dyes have emerged as exceptionally useful probes for biological imaging.[16–19] Replacing the oxygen atom in xanthene with an Si moiety results in a bathochromic shift of ~100 nm, which can prevent self-quenching due the excitation light and benefit the testing process. Unfortunately, no fluorescent dye with a large Stokes shift (>150 nm) has been adopted in the labelling of IgG antibodies. Herein, we designed three Si–rhodamine (SiRh) analogues, and applied them to IgG antibody labelling. Selectivity tests with SARS-CoV-2 were also performed.

As illustrated in Fig. 1a, three Si–rhodamine analogues were easily synthesized *via* several steps with acceptable yields (ESI†). All the SiRh analogues as well as the intermediates were characterized using ^{1}HNMR, ^{13}CNMR and HRMS (Fig. S10–S43†). The photophysical properties of SiRh analogues were studied first. As illustrated in Fig. 1b–d and S1–S6,† all of the fluorescence emissions of these SiRh analogues were from red to NIR wavelengths. Meanwhile, all of these SiRh analogues exhibited large Stokes shifts of over 140 nm, indicating the great potential application in avoiding self-quenching caused by backscattering from biological samples in antibody-labelling fields. Furthermore, the fluorescence intensities of these dyes in various solutions of different pH levels were also measured. As shown in the Fig. S7,† all of the dyes displayed very slightly decreased intensities from pH 3–7, and these dyes showed obvious decreased fluorescence intensity when the pH was over 8. Quite importantly, the fluorescence spectrum of these new synthesized dyes in the presence of GSH were measured. Hardly any fluorescence quenching was observed when GSH was included in the test solution (Fig. S8†), indicative of great anti-interference ability. Subsequently, the absolute quantum yields of these compounds were also characterized. **P-Si-ARh** in PBS buffer showed an absolute quantum yield (QY) of 0.22, the highest of the tested compounds. The higher QY observed for **P-Si-ARh** was due to the suppressive TICT effects known to be displayed by its pyrrole group. It also showed brighter fluorescence than that of the traditional Si–rhodamine. A comparison of optical properties of traditional Si–rhodamine and the dyes constructed in the current work is shown in the Table S1.†

It appeared obvious that the excellent brightness displayed by **P-Si-ARh** could play a major role in IgG antibody labelling and in testing of SARS-CoV-2. Hence, we chose **P-Si-ARh** as the core structure for further experiments, with the maleimide group as the labelling group.

First, we chose the commercial donkey-anti-rabbit IgG antibody for the labelling experiments. This antibody was dissolved in PBS buffer (pH = 7.4) to prepare the IgG antibody solution (1 mg mL$^{-1}$) and the **P-Si-MRh** probe was dissolved in DMSO to prepare for the probe solution (1 mg mL$^{-1}$). We tested various labelling ratios between IgG antibody and **P-Si-MRh** and various dilution ratios. As shown in Fig. S9,† the best labelling efficiency was observed when the mass concentration ratio between IgG antibody and **P-Si-**

**MRh** was 4/1 and the dilution ratio was 1/10. Using this mass concentration ratio, we further examined the degree of labelling, determined using UV-vis spectroscopy. The degree of labelling was calculated to be 1.16, indicating that each IgG antibody was labelled with a fluorescent dye. Subsequently, we acquired fluorescence and circular dichroism spectra before and after the labelling. As shown in Fig. 2b, both the fluorescence and circular dichroism spectra changed very little upon labelling with probe, indicative of little effect of labelling on the structures of the IgG antibody and fluorescent dye. These results provided confidence in our ability to interpret the results of our subsequent experiments. The determination of SARS-CoV-2 exposure relies largely on the detection of either IgM or IgG antibodies that are specific for various viral antigens including, but not exclusively, the spike glycoprotein (S1 and S2 subunits, receptor-binding domain) and nucleocapsid protein. The available methodologies used for these determinations include the traditional enzyme-linked immunosorbent assay (ELISA), immunochromatographic lateral flow assay, neutralization bioassay, and specific chemosensors.[7] Each of these formats shows advantages (speed, multiplexing, automation) and disadvantages (need for trained personnel, dedicated laboratories). Tests complementary to these antibody-detecting methods are the rapid antigen tests wherein antibodies are used to detect the presence of viral antigen in serological samples. Development of high-throughput serology tests is a current focus of major diagnostic companies. Also, fluorescence enzyme-linked immunosorbent assays rely on the fluorescence output, which depend on the fluorescence properties of the fluorescent dyes used. In
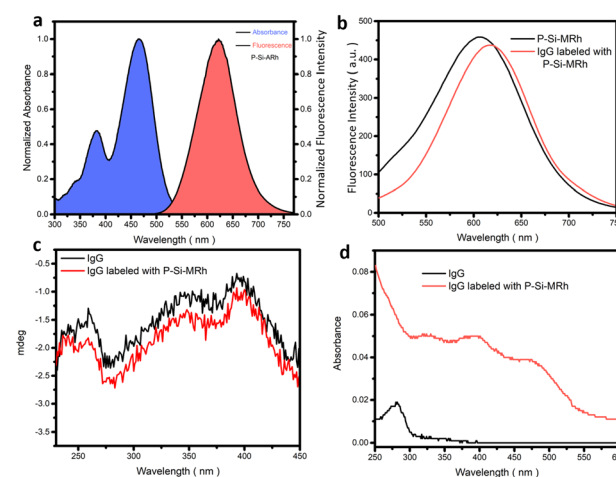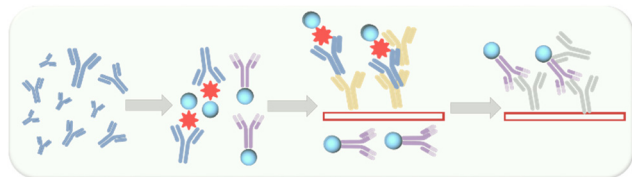


**Fig. 2** (a) Normalized absorbance spectrum and fluorescence spectrum of **P-Si-MRh** (10 mM in PBS 7.4). (b) Fluorescence spectra of **P-Si-MRh** before after being its labelling of IgG (1 mg mL$^{-1}$ in PBS 7.4). (c) Circular dichroism spectra of IgG before and after being labelled with **P-Si-MRh** (1 mg mL$^{-1}$ in PBS 7.4). (d) Absorbance spectra of IgG before after being labelled with **P-Si-MRh** (1 mg mL$^{-1}$ in PBS 7.4).

**Scheme 1** Schematic presentation of the ELISA-method-based detection of SARS-CoV-2 by **P-Si-MRh**-labelled IgG antibody (1 mg mL⁻¹ in PBS 7.4).

this manner, we utilized the Si-MARh-labelled IgG antibody to investigate the efficiency of detecting SARS-CoV-2 as illustrated in Scheme 1.

The angiotensin-converting enzyme 2 (ACE2) receptor is an important cytomembrane receptor shown to play a key role in SARS-CoV-2 virus infection.[20] It is widely distributed in a variety of tissues including heart, lung, gut, kidney, testis and brain.[20] Gene expression of ACE2 in DU145, HepG 2, HeLa and Skov-3 cells was investigated by carrying out reverse-transcription polymerase chain reaction (RT-PCR) assays. For RNA extraction, the cells were harvested and washed twice with PBS. Total RNA was extracted using Trizol reagent. The concentration of RNA was measured using a SimpliNano reader (GE). Gene levels of ACE2 in the different types of cells was analysed using a one-step RT-PCR kit (TAKARA) following the standard procedure. The gene for glyceraldehyde 3-phosphate dehydrogenase (GADPH) was used as a reference gene. Relative expression of ACE2 mRNA was normalized to GADPH mRNA. As seen in Fig. 3d, ACE2 exhibited higher gene expression levels in SKOV-3 and HeLa cells than in DU145 and HepG2 cells. Simultaneously, the fluorescent IgG labelled by the large-Stokes-shift dye **P-Si-MRh** was used in an immunostaining assay to evaluate the protein expression levels of ACE2 in DU145, HepG2, HeLa and Skov-3 cells. To analyse ACE2 protein expression in the different types of cells *in situ*, the cells were fixed with 4% paraformaldehyde for 30 minutes at room temperature and blocked with 5% bovine serum albumin (BSA) at 37 °C for 1 h. Fixed cells were incubated with rabbit anti-human ACE2

antibody (1 : 2000) overnight at 4 °C. After washing thrice with phosphate-buffered saline, the **P-Si-MRh** conjugated donkey anti-rabbit secondary antibody (1 : 20) was added into the cells and incubated at 37 °C for 1 h. **P-Si-MRh**-labelled fluorescent IgG displayed high specificity and sensitivity to target protein. In the immunostaining test, images with high signal-to-noise ratios were obtained owing to the excellent optical properties, namely strong fluorescence intensity and large Stokes shift, of **P-Si-MRh**. As shown in Fig. 3a, strong fluorescent staining was observed in the cytomembranes of Skov-3 and HeLa cells. However, only weak fluorescence signals were found for the DU145 and HepG2 cells. These results showed an obvious difference between the ACE2 protein levels of the four cell lines, in agreement with gene expression detection using RT-PCR. To further test the Immunofluorescence imaging ability of **P-Si-MRh**, it was used to image F-actin. As shown in the Fig. S10,† the fluorescence signal was intense and the morphology of F-actin was clear, showing an ideal immunofluorescence imaging ability.

Entry of SARS-CoV-2 virus into host cells is mediated by the *trans*-membrane spike (S) glycoprotein. S protein is composed of two functional subunits: S1 and S2. The S1 subunit is involved in recognizing and binding the ACE2 receptor on host cell membrane. The S2 subunit is involved in mediating fusion of the virus with the host cell membrane.[20] In antiviral research, the S1 subunit is used as a key target to respond to neutralizing antibodies and protect against viral infection. To assess the binding process of the S1 subunit and ACE2 receptor in the cell membrane, Skov-3 cells were incubated with S1 for a series of times and then **P-Si-MRh**-labelled fluorescent IgG was used to perform a special staining *in situ*. Cells were incubated with spike S1 protein for 4 h, 18 h and 24 h, respectively. Immunostaining was then performed as described above with minor modifications. Fixed SKOV-3 cells were treated with rabbit anti-human spike S1 and **P-Si-MRh**-labelled goat anti-rabbit secondary antibody. Nuclei were stained with Hoechst 3342 and cells were imaged with laser scanning confocal microscopy. As shown in Fig. 4, after incubation for 18 h, weak fluorescence was observed. It revealed that few spike S1
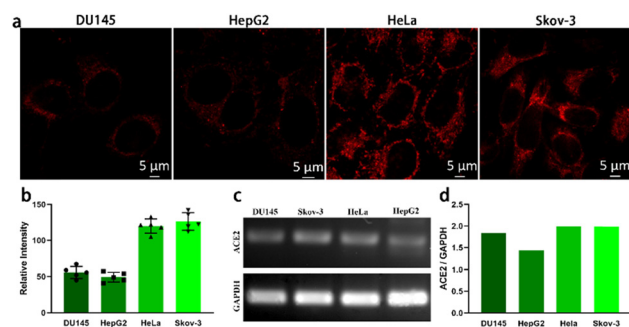


**Fig. 3** (a) Immunofluorescence images of samples of ACE2 protein in DU145, HepG2, HeLa and Skov-3 cells, respectively. (b) Plot of average fluorescence intensities derived from the fluorescence images in panel (a). (c) Gene expression of ACE2 in each of four kinds of cells. (d) Plot of the relative expression levels of ACE2 derived from panel c.
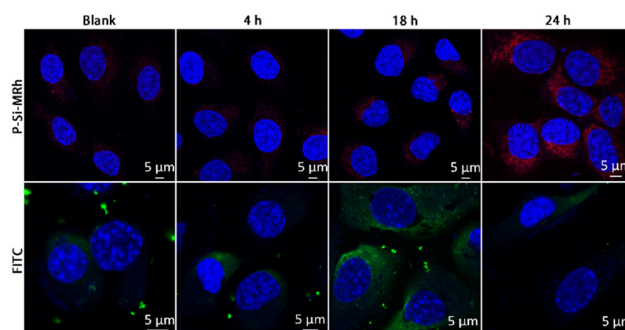


**Fig. 4** Immunofluorescence images of spike S1 protein in samples of Skov-3 cells labelled with, respectively, **P-Si-MRh** and FITC at indicated incubation times.
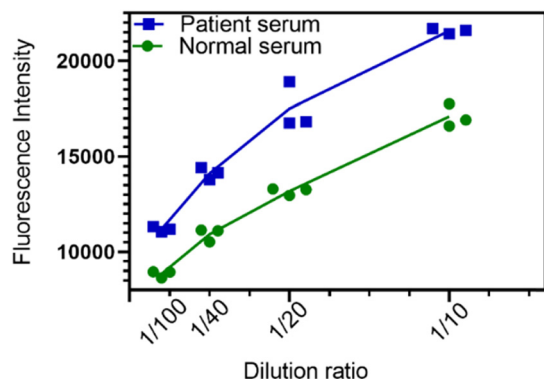
**Fig. 5** Plots showing differences between patient serum and normal serum based on fluorescent **P-Si-MRh**-labelled IgG under indicated dilution ratios.

proteins were trapped by ACE2 receptor. At 24 h, fluorescence intensity markedly increased. Some binding of the S1 subunit to the ACE2 receptor was detected. Cells were immunostained using **P-Si-MRh**-labelled fluorescent IgG and imaged using confocal microscopy. These images showed higher resolution and lower nonspecific adsorption than did those of commercial FITC-conjugated fluorescent IgG.

To investigate detection, a fluorescence-linked indirect immunosorbent (FLISA) method was developed using **P-Si-MRh**-labelled fluorescent IgG as secondary antibodies instead of traditional HRP-linked antibodies. Due the procedure involving the chromogenic reaction being omitted, the detection time was effectively shortened in this fluorescence method. Spike S1 protein-specific antibody response to SARS-CoV-2 infection was evaluated both in healthy and patient donor sera (Fig. 5). Compared to healthy sera, in COVID-19 patient sera samples showed significantly higher spike-S1-specific antibody levels even at a dilution of 1 : 400. The fluorescence intensity was positively associated with sample dilution ratio. In addition, owing to the attractive optics properties of **P-Si-MRh**, there was no interference between the excitation and emission wavelengths in the detection process by the microplate reader even at a bandwidth larger than 18 nm. Taken together, a sensitive and rapid fluorescence immunosorbent method based on **P-Si-MRh** labelling of IgG was developed and successfully applied in the detection of spike S1 protein-specific IgG against SARS-CoV-2.

In summary, we developed a series of new Si–rhodamine analogues. These fluorescent dyes exhibited obviously improved Stokes shifts, and highly stable and anti-interference ability characters. Nucleophilic biological species such as GSH did not quench the fluorescence signal, providing great promise for the antibody labelling—in contrast to the widely used fluorescent dyes such as FITC, RRX, Cy3(5), and PE, which show small Stokes shifts and are easily interfered with by GSH in serum, resulting in false-signal outputs. Especially **P-Si-ARh** with its high absolute quantum yield could play a major role in IgG antibody

labelling and tests of SARS-CoV-2. Finally, this **P-Si-ARh**-constructed ELISA-based detection method succeeded in distinguishing normal serum from that of COVID-19 patients. However, the utilization of these dyes in immunofluorescent staining and imaging in organs may not perform as well as in cells or test tubes due to the short fluorescence emission wavelength causing an insufficient depth of penetration. For immunofluorescence staining of organs, highly stable NIR II fluorescent dyes displaying large Stokes shifts remain highly desired. Nevertheless, these newly developed highly stable large-Stokes-shift fluorescent dyes could constitute an outstanding toolbox for antibody labelling in biological domains in cells and test tubes.

## Conflicts of interest

The authors declare no competing financial interest.

## Acknowledgements

## Notes and references

1 D. Mannar, J. W. Saville, C. Poloni, X. Zhu, A. Bezeruk, K. Tidey, S. Ahmed, K. S. Tuttle, F. Vahdatihassani, S. Cholak, L. Cook, T. S. Steiner and S. Subramaniam, *Nat. Commun.*, 2024, **15**, 1854.

2 M. A. Sadique, S. Yadav, R. Khan and A. K. Srivastava, *Chem. Soc. Rev.*, 2024, **53**, 3774–3828.

3 S. Delgado, P. Somovilla, C. Ferrer-Orta, B. Martínez-González, S. Vázquez-Monteagudo, J. Muñoz-Flores, M. E. Soria, C. García-Crespo, A. I. de Ávila, A. Durán-Pastor, I. Gadea, C. López-Galíndez, F. Moran, R. Lorenzo-Redondo, N. Verdaguer, C. Perales and E. Domingo, *Proc. Natl. Acad. Sci. U. S. A.*, 2024, **121**, e2317851121.

4 Z. Liao, C. Wang, X. Tang, M. Yang, Z. Duan, L. Liu, S. Lu, L. Ma, R. Cheng, G. Wang, H. Liu, S. Yang, J. Xu, D. A. Tadese, J. Mwangi, P. M. Kamau, Z. Zhang, L. Yang, G. Liao, X. Zhao, X. Peng and R. Lai, *Proc. Natl. Acad. Sci. U. S. A.*, 2024, **121**, e2317026121.

5 B. D. Kevadiya, J. Machhi, J. Herskovitz, M. D. Oleynikov, W. R. Blomberg, N. Bajwa, D. Soni, S. Das, M. Hasan, M. Patel, A. M. Senan, S. Gorantla, J. McMillan, B. Edagwa, R. Eisenberg, C. B. Gurumurthy, S. P. M. Reid, C. Punyadeera, L. Chang and H. E. Gendelman, *Nat. Mater.*, 2021, **20**, 593–605.

6 A. Domling and L. Gao, *Chem*, 2020, **6**, 1283–1295.

7 J. Watson, A. Richter and J. Deeks, *BMJ*, 2020, **370**, m3325.

8 Y. Finkel, O. Mizrahi, A. Nachshon, S. Weingarten-Gabbay, D. Morgenstern, Y. Yahalom-Ronen, H. Tamir, H. Achdout, D. Stein, O. Israeli, A. Beth-Din, S. Melamed, S. Weiss, T. Israely, N. Paran, M. Schwartz and N. Stern-Ginossar, *Nature*, 2021, **589**, 125–130.

9   C. Bundschuh, M. Egger, K. Wiesinger, C. Gabriel, M. Clodi, T. Mueller and B. Dieplinger, *Clin. Chim. Acta*, 2020, **509**, 79–82.

10  E. A. Meyerowitz, J. Scott, A. Richterman, V. Male and M. Cevik, *Nat. Rev. Microbiol.*, 2024, **22**, 75–88.

11  D. Kim, J. Y. Lee, J. S. Yang, J. W. Kim, V. N. Kim and H. Chang, *Cell*, 2020, **181**, 914–921, e910.

12  F. Gong, H. X. Wei, J. Qi, H. Ma, L. Liu, J. Weng, X. Zheng, Q. Li, D. Zhao, H. Fang, L. Liu, H. He, C. Ma, J. Han, A. Sun, B. Wang, T. Jin, B. Li and B. Li, *ACS Sens.*, 2021, **6**, 2709–2719.

13  Y. Liu, Y. Tan, Q. Fu, M. Lin, J. He, S. He, M. Yang, S. Chen and J. Zhou, *Biosens. Bioelectron.*, 2021, **176**, 112920.

14  Z. Li, Y. Yi, X. Luo, N. Xiong, Y. Liu, S. Li, R. Sun, Y. Wang, B. Hu, W. Chen, Y. Zhang, J. Wang, B. Huang, Y. Lin, J. Yang, W. Cai, X. Wang, J. Cheng, Z. Chen, K. Sun, W. Pan, Z. Zhan, L. Chen and F. Ye, *J. Med. Virol.*, 2020, **92**, 1518–1524.

15  C. L. Schreiber, D.-H. Li and B. D. Smith, *Anal. Chem.*, 2021, **93**, 3643–3651.

16  A. N. Butkevich, G. Lukinavicius, E. D'Este and S. W. Hell, *J. Am. Chem. Soc.*, 2017, **139**, 12378–12381.

17  A. Morozumi, M. Kamiya, S. N. Uno, K. Umezawa, R. Kojima, T. Yoshihara, S. Tobita and Y. Urano, *J. Am. Chem. Soc.*, 2020, **142**, 9625–9633.

18  H. Zhang, L. Shi, K. Li, X. Liu, M. Won, Y.-Z. Liu, Y. Choe, X.-Y. Liu, Y.-H. Liu, S.-Y. Chen, K.-K. Yu, J. S. Kim and X.-Q. Yu, *Angew. Chem.*, 2022, **61**, e202116439.

19  H. Zhang, F.-F. Xiang, Y.-Z. Liu, Y.-J. Chen, D.-H. Zhou, Y.-H. Liu, S.-Y. Chen, X.-Q. Yu and K. Li, *JACS Au*, 2023, **3**, 3462–3472.

20  A. Malhotra, M. Hepokoski, K. C. McCowen and J. Y.-J. Shyy, *iScience*, 2020, **23**, 101425.